

<https://doi.org/10.1038/s44385-025-00016-y>

Automated microinjection for zebrafish xenograft models

Check for updates

Yi Ding^{1,8}, Kees-Jan van der Kolk^{1,8}, Wietske van der Ent², Michele Scotto di Mase³, Saskia Kowald⁴, Jenny Huizing⁵, Jana M. Vidal Teuton⁵, Gunja Mishra⁵, Maxime Kempers¹, Rusul Almeter⁴, Sandra Kunz², Laurine Munier², Carl Koschmann⁶, Sebastian M. Waszak², Vincenzo Di Donato³, Sylvia Dyballa³, Peter Ten Dijke⁵, Camila Vicencio Esguerra², Lasse D. Jensen^{4,7} & Jan de Sonnevile¹ ✉

Zebrafish xenograft models are increasingly recognized for predicting patient responses to cancer therapeutics, suggesting their potential as clinical diagnostic tools. However, precise microinjection of cancer cells into numerous small and fragile zebrafish larvae is laborious, requires extensive training for new operators, and often yields variable results, limiting their clinical and drug discovery applications. To address these challenges, we have designed, built, and validated an automated microinjection robot. The robot performs injections into the vasculature, perivitelline space, and hindbrain ventricle in both fully automated and semi-automated modes. Combined results demonstrate an average injection success rate of approximately 60% and larvae survival exceeding 70%, comparable to manual methods, with the fully automated mode being twice as fast. This automation reduces the need for extensive personnel training while enhancing reproducibility, efficiency, and accuracy, paving the way for more extensive use of zebrafish xenograft models in drug discovery and patient diagnostics.

Over the past decades, the zebrafish (*Danio rerio*) has emerged as a powerful vertebrate model organism for studying various human diseases, including cancer^{1,2}. The introduction of human cells into zebrafish larvae, i.e., xenograft transplantation, is a widely employed technique to study tumor behavior in vivo, offering a dynamic and versatile model for cancer research^{3,4}. Zebrafish larvae offer unique advantages over cell cultures and mammalian models in tumor research: their small size, high yield, transparency, tolerance for xenografts, the small number of cells required for implantation, and the rapid growth of xenografts. Zebrafish xenograft models have been used effectively to investigate processes such as tumor formation, migration, metastasis, intravasation, and extravasation^{5,6}. Various cancer cell lines, including those from prostate cancer⁷, breast cancer⁸, urinary bladder cancer⁹, colorectal cancer¹⁰, glioblastoma¹¹, and pediatric brain tumors¹² have been shown to form tumors, proliferate, and/or extravasate in zebrafish. Additionally, the zebrafish patient-derived xenograft (PDX) model has gained traction as a promising model for predicting individual treatment responses and clinical outcomes in patients with colorectal¹³, pancreatic¹⁴, epithelial ovarian cancer¹⁵, non-small cell lung cancer¹⁶, and rectal cancer¹⁷.

Microinjection is a critical technique for introducing exogenous substances into zebrafish larvae for disease studies, such as cancer and infections. Zebrafish larvae present multiple sites, which are well-tolerated injection locations including the duct of Cuvier (DoC), the perivitelline space (PVS), and the hindbrain ventricle. Systemic injection via the DoC allows the introduction of the injected material directly into the bloodstream. This facilitates the in vivo evaluation of various stages of tumorigenesis, such as migration, intravasation, extravasation, and metastatic outgrowth at distant sites in cases where tumor cells are injected^{18–21}. Once in the bloodstream, different cancer cell subtypes, albeit inefficiently, survive, and intravasate in the tail region, with labeled cells being trackable and quantifiable²². The PVS, located between the periderm and the yolk syncytial layer, is another commonly used injection site²³. The avascular nature of the PVS makes it ideal for studying newly formed blood vessels and further exploring migration, metastatic behavior, and tumor intravasation efficiency^{21,24,25}. The hindbrain ventricle is also an intriguing site. Injection of human melanoma cells and breast cancer cells into the hindbrain ventricle of zebrafish larvae has resulted in the formation of tumor masses and new vessels in the brain region^{26,27}. Additionally, the transplantation of

¹Life Science Methods BV, Leiden, the Netherlands. ²Centre for Molecular Medicine Norway (NCMM), University of Oslo, Oslo, Norway. ³ZeClinics SL, Barcelona, Spain. ⁴BioReperia AB, Linköping, Sweden. ⁵Oncode Institute, Dept. Cell & Chemical Biology, Leiden University Medical Center, Leiden, the Netherlands. ⁶Department of Pediatrics, University of Michigan, Ann Arbor, MI, USA. ⁷Division of Diagnostics and Specialist Medicine, Linköping University, Linköping, Sweden. ⁸These authors contributed equally: Yi Ding, Kees-Jan van der Kolk. ✉e-mail: jan@lifesciencemethods.com

glioblastoma cells into this site has shown increased tumor area, proliferation, migration, and responsiveness to chemotherapeutics^{28,29}.

Despite the invaluable insights derived from injections at these anatomical sites, the process of microinjection remains a laborious task, especially for researchers who lack experience with these techniques. Conventionally, microinjection has been conducted across research laboratories worldwide using manual systems consisting of a stereo dissecting microscope, an air-pressure-based microinjector, and a micromanipulator^{30,31}. This manual approach presents challenges, primarily due to the small size of 2-day post-fertilization (dpf) zebrafish larvae, which measure approximately 3.7 mm in length and 0.6 mm in width³². Additional challenges include the minimal needle tip size to fit cancer cells and the complexities associated with targeting specific injection sites without causing overt damage to the larvae. Consequently, this manual process demands extensive training and practice, requires substantial time to perform the injections, and, therefore, has limited throughput capacity. Even after extensive training, variability in experimental results persists among researchers, arising from differences in skill levels, cognitive abilities, protocol interpretation, instrument usage, and environmental conditions.

These technical challenges hinder the adoption of zebrafish xenotransplantation models for fast-turnover screening of compound efficacy for patient tumor treatment or drug discovery. Therefore, automatization of the injection process would accelerate the pace of tumor progression assessment and contribute to the timely assessment of therapeutic intervention. Some research groups have made efforts to innovate larvae preparation^{33,34} and the design of robotic microinjection systems^{32,35,36}. However, such systems were not validated with xenograft assays, nor tested by life sciences researchers. While aqueous liquids are relatively simple to inject due to the low viscosity and high homogeneity of the liquids, injecting living cells represents an enormous challenge. Cells are large, for example, the breast cancer cells MDA-MB-231 have a size range of 15–25 μm , requiring significantly larger diameters of the injection needles, which in turn may lead to more damage and reduced survival of the larvae. Furthermore, cells are likely to sediment, clump together, and may be more temperature- and/or time-sensitive compared to injection of non-viable biological material. This can result in higher and heterogeneous viscosity, fluidity, and therefore variable injection volume at constant pressure.

In this study, as part of the Eurostars consortium ROBO-FISH project, Life Science Methods (LSM) designed and developed a specialized robotic system for zebrafish larvae xenotransplantation procedures. The injection robot was subsequently tested and validated by injection of various substances and cancer cells at multiple laboratories of start-ups and institutions across Europe. These include Bioreperia in Sweden, the Center for Molecular Medicine Norway (NCMM) in Norway, LSM and Leiden University Medical Center (LUMC) in the Netherlands, and ZeClinics in Spain. Results from multiple labs showed an average injection success rate of approximately 60% and a survival rate exceeding 70% for the three injection sites of 2 dpf zebrafish larvae using the robot. These outcomes are highly comparable to manual injections using a traditional micromanipulator. Moreover, the fully automated mode of the robot was, on average twice, as fast as manual injections. Therefore, the robot accelerates the injection process, simplifies this challenging task, and reduces labor intensity, allowing higher throughput. This facilitates the uptake of zebrafish tumor xenograft models at new sites, potentially even at sites with minimal or no prior experience with zebrafish work, such as cancer clinics.

Results

Overview of the design of the injection robot for zebrafish larvae

To accommodate microinjections at various anatomical sites, we have designed a robot as depicted in Fig. 1A. This system comprises several components to facilitate precise and adaptable injection processes. From the top cross-sectional perspective, we have incorporated a camera (acA1920-40uc, Basler AG, Germany) equipped with a high-resolution 10 \times telecentric lens with liquid focus (VS-TM10-55CO-LQL1, VST Europe B.V., the Netherlands), enabling detailed visualization of the injection procedures from

above. To switch focus between the needle tip and the sample below, an Optotune liquid lens with an increased range was used (EL-16-40-TC-VIS-20D, Optotune Switzerland AG). In the middle section of the robot, the needle is affixed to a holder capable of rotation around the upper lens (Supplementary Movie 1). This permits adjustment of the needle orientation to the target, a departure from the conventional approach of manipulating the sample or sample holder to match the needle orientation. The lower section of the system employs a camera (acA4024-29um, Basler AG, Germany) in conjunction with a 0.5 \times telecentric lens (VS-TCT05-65CO/S, VST Europe B.V., the Netherlands) to facilitate the detection of subsequent zebrafish larvae for injection. For illumination, a dome light, emitting broad rays of light, is employed to produce high numerical aperture (NA) lighting, resulting in a minimal depth of view as observed from the top-camera perspective, thereby enhancing surface focus (Supplementary Movie 2). Additionally, a coaxial light source utilizes the input of the bottom lens to generate parallel, low-NA light, effectively increasing the depth of field (Supplementary Movie 3) for the top camera. This feature proved invaluable, for instance, in the examination of intricate structures such as zebrafish blood flow. Figure 1B shows an image of the front side of the robot, presenting the fully integrated product. The injector is built into the robot, which is connected to a power adapter (48 V; 280 W) and compressed air (6 MPa) (not shown). At the top, the black cylinder contains the camera, lenses, and a motor for rotating the needle at various angles. In the middle, two plates are located on the motorized stage: one 6-well plate for droplet calibration and an agarose gel plate for placing zebrafish larvae. At the bottom, there is a power button and a touch screen. The touch screen is used for the operation of the system and observation of the injection procedure in real time.

Robotic injection procedure and puncture detection

The injection procedure for zebrafish larvae comprises five steps: injection settings, needle calibration, droplet calibration, plate selection, and injection. The procedure begins with configuring the injection settings, which include selecting different developmental stages, injection sites, injection locations with a specific needle starting point and angle as well as injection macros (Fig. 2A and Supplementary Movie 4). In the settings for injection sites, ‘duct of Cuvier’ refers to injections performed at the middle of the DoC. In contrast, ‘duct of Cuvier (choose point)’ means that injections can be performed at any point along the DoC (Supplementary Movie 4). In full-automatic mode, the injection macro corresponding to the selected injection site can be chosen (Supplementary Movie 4). The robot will scan the agarose plate, approach each zebrafish larva and its predetermined injection site, perform the injection macro, and then proceed to the next larva automatically. In semi-automatic mode, users can select the ‘manual’ injection macro (Supplementary Movie 4). In this mode, the robot positions the zebrafish larvae and navigates to the selected injection site, while allowing users to manually control the needle for injections. Next, needle calibration is performed to ensure the needle is at the correct height and validate the injection point of each rotation. This is achieved by adjustment of needle length and yaw (x , y) on the needle holder and focus (z) of the top camera using three screws on the robot (Fig. 2B and Supplementary Movie 5). The droplet size is then automatically measured in mineral oil within a 6-well plate. Injection pressure settings can be adjusted to achieve the desired volume (Fig. 2C and Supplementary Movie 6). In the plate selection interface, the stage can be moved into position to receive an agarose gel plate with around 20 anesthetized zebrafish larvae; these are randomly distributed (Fig. 2D, E). The operator does not need to pre-arrange and orient the larvae according to different injection sites, as the robot will automatically recognize the larvae’s orientation and adjust the needle to the predetermined angle that fits the larvae’s orientation. Finally, the injection process can commence (Fig. 2F). To enable the robot to recognize the zebrafish larvae, thousands of images were collected and annotated (Supplementary Fig. 1). This extensive dataset allows the larvae on the agarose plate to be accurately detected after the machine learning model is trained on the annotated zebrafish images (Fig. 2G). The injection process begins with the robot scanning the agarose plate to locate a larva (Fig. 2H). Once a larva is identified, the needle automatically navigates to the designated

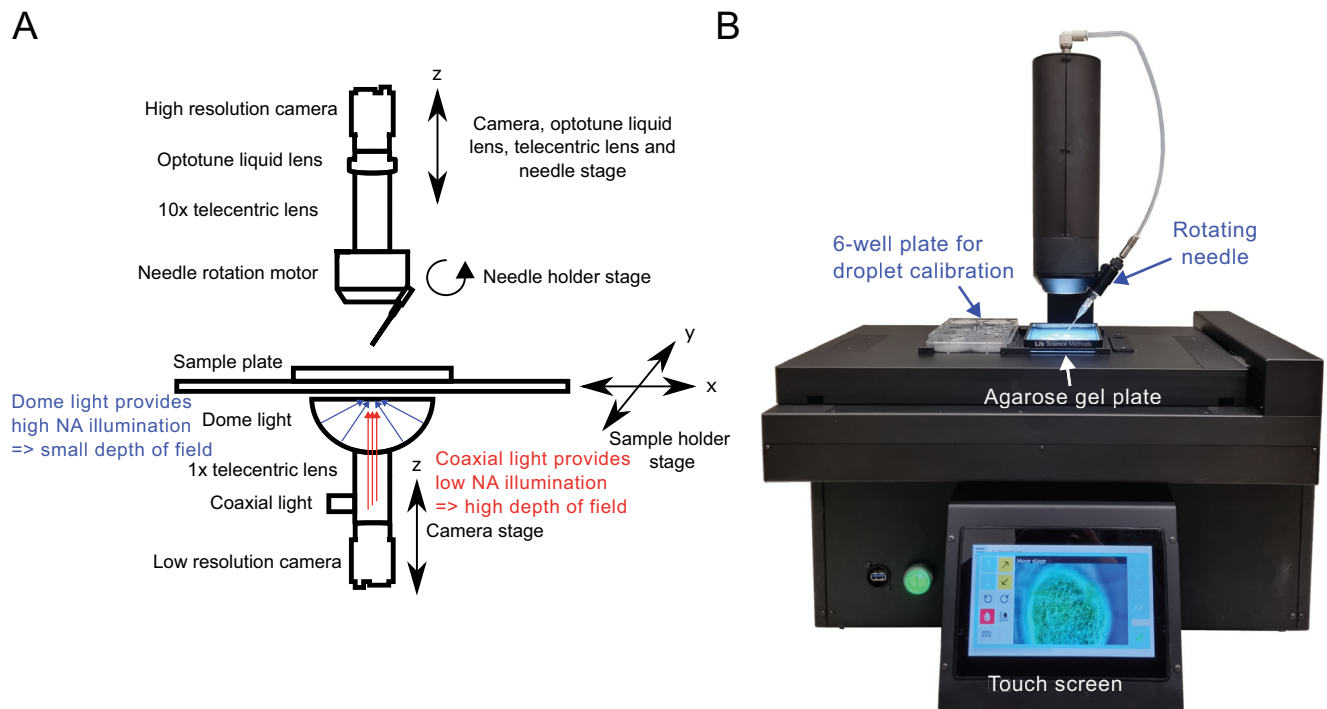


Fig. 1 | Design and visualization of the automated injection robot for zebrafish larvae. **A** Schematic diagram illustrating the design and key components of the automated injection robot. **B** Photograph showing the fully assembled automated injection robot in operation. Dimensions: 42 × 50 × 42 cm (wide × height × depth).

injection site. Using the liquid lens, the focus of the top camera is set to below the needle, and the head is lowered until the autofocus finds the larva. Subsequently, the focus is switched to the needle tip, and the approach continues until a touchdown is detected. Then, the injection macro is started if the automated mode is selected (Fig. 2H). If not, the user can now take over control to guide an injection, which is the semi-automated mode. One strategy to detect puncture of the skin was to monitor the movement of labeled anchor points around the needle-tip (Fig. 2I and Supplementary Movie 7). Each anchor point is connected to a few pixels in the image; these are tracked, frame by frame. As the needle pushes the skin, the points move collectively in small increments. However, during puncture, a larger movement can be detected when the skin retracts more rapidly. Below, we show detailed injection results from three injection sites: DoC, perivitelline space, and hindbrain ventricle.

Injections into the DoC of zebrafish larvae

The DoC, also known as the common cardinal vein, is a major venous structure with extensive blood flow in zebrafish larvae. It is a broad conduit on the embryonic yolk sac that collects blood from the anterior and posterior cardinal veins and directs it to the heart (Fig. 3A). This vein allows for the direct injection of substances into the bloodstream. In the injection settings, the needle tip can be positioned anywhere within the DoC area with flexibility in angle selection. Figure 3B is an example where the needle is placed at the center of the DoC, aligned against the direction of blood flow, and made visible by use of coaxial illumination. Since a static image cannot capture flowing blood, a short video consisting of 10 frames was recorded, highlighting differences in red to make the blood flow clearly visible, see Fig. 3C. The DoC region of 2 dpf zebrafish larvae was annotated, and a machine-learning model was trained on thousands of annotated images of DoC (Fig. 3C). Consequently, the robot can accurately recognize the shape of the DoC (Fig. 3C). Various substances, including dyes (trypan blue, dextran, and phenol red), tumor-infiltrating lymphocytes (TILs), the human bladder cancer cell line UM-UC-3, microspheres, and the human breast cancer cell line MDA-MB-231, were injected into the DoC of 2 dpf zebrafish larvae to validate the robot across four independent labs in Europe. In the automated mode, larvae are injected in a fully automatic manner. The injection site is

positioned in the middle of the DoC, and the substance is clearly visible, entering the bloodstream immediately (Supplementary Movie 8). For suspensions that contain small particles, e.g., dyes, a droplet size measurement in oil is representative of the injected volume (Supplementary Fig. 2). In the semi-automated mode, the robot recognizes and approaches the larvae automatically, and users have the flexibility to control the needle, adjust the focus, and perform the injection using the touchscreen. The injection site is chosen on the border of the yolk for larger substances like MDA-MB-231 cells (Supplementary Movie 9). This is because the DoC layer is so thin that the cells are more likely to be injected into the yolk. For large cancer cells, the calibrated droplet is not always representative of the injected volume due to the cells sedimenting in the needle, and also, one large pulse often results in a larger spread in the embryo, e.g., in the yolk. Therefore, for some cancer cells, multiple droplets are injected to reach the desired size of implantation, which is visually observed during the injection (Supplementary Movie 9). As shown in Fig. 3D and the three-dimensional reconstructed video in Supplementary Movie 10, the injected substances were well distributed in the bloodstream of zebrafish larvae. Furthermore, the common manual injection method using a micromanipulator was performed by skilled researchers for comparison with the robotic injections. Detailed data about the injection time, success rate, and survival rate for the injections into the DoC are presented in Fig. 3E. The injection of dyes and TILs using both modes of the robot achieved success rates exceeding 70% at both Bioreperia and ZeClinics, while manual injections of dyes at Bioreperia had a success rate of 50%. At NCMM, the success rates for robotic and manual injections of microspheres were 54% and 47%, respectively. For cancer cell injections, the success rate of the robotic method ranged from 53% to 61%, slightly lower than the 70% success rate of the manual method. Overall, the average success rates for both modes of the robot (63% and 71%) were higher than that of the manual injector (56%). The injection time per larva using the automated mode (43 s) was approximately half that of manual injections (84 s). Consequently, the average number of larvae injected within a given period was twice as high with the automated injection compared to manual injection. The manual injection rate is highly variable and dependent on the experience of different researchers. In contrast, the robotic injection rate is much less dependent on the individual performing the procedure. Although the survival rate for robotic injections was

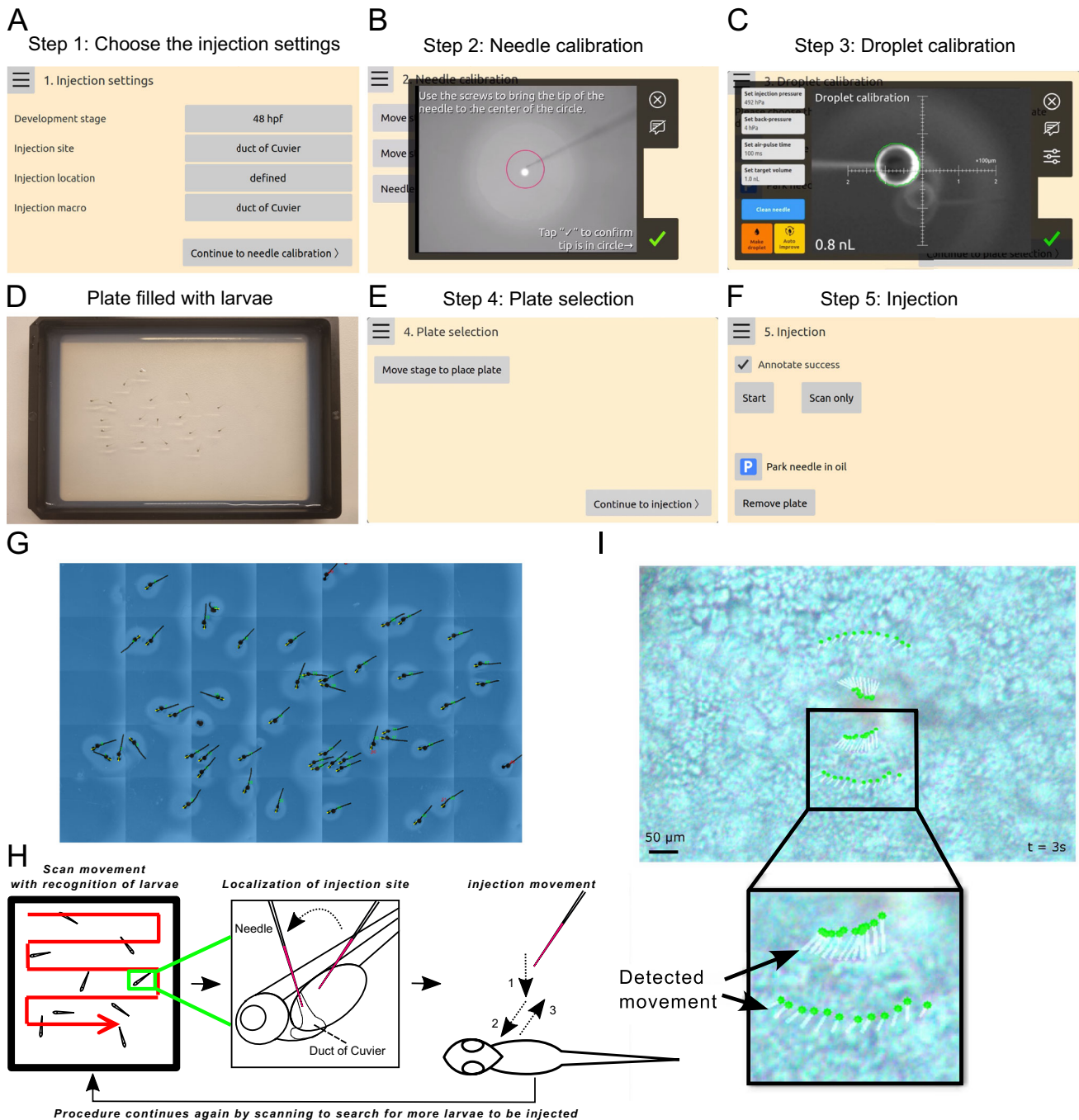


Fig. 2 | The injection procedure of the robotic injection system for zebrafish larvae. **A** Various injection settings can be selected, including the developmental stage, injection site, injection location on schematic drawing, and injection macro. **B** Calibration of the needle is performed in the x, y, and z directions in semi-automated mode. **C** The volume of the injection droplet is automatically measured in a well filled with mineral oil. **D** Prepare a 1.5% agarose gel plate and randomly place the anesthetized zebrafish larvae on the agarose gel plate. **E** Click “Move stage to place plate” and the robot will automatically move the stage to the correct position for placing the plate with the

anesthetized larvae on the designated holder. **F** In the injection interface, click the “Start” button to begin the injection process. The “Scan only” button enables scanning and image collection of zebrafish larvae for annotations. The “Park needle in oil” option allows the needle to rest in oil, preventing dryness and blockage. **G** Zebrafish larvae are automatically detected by the robot after training the algorithm. **H** The injection procedure involves scanning the plate to locate a larva, approaching the larva, and executing the injection macro if the automatic mode is selected. **I** Skin puncture by the needle is detected through the movement of the marked anchor points.

slightly lower than that for manual injections, this discrepancy was primarily due to an outlier in the UM-UC-3 cell injection data.

Injections into the perivitelline space of zebrafish larvae

The perivitelline space (PVS) is an avascular area located between the periderm and the yolk syncytial layer (Fig. 4A). For injection settings, it is recommended to position the needle tip at the upper border of the PVS with

an angle of around 30–60° (Fig. 4B). To enable the robot to recognize the PVS structure, numerous images of the PVS area of 2 dpf zebrafish larvae were collected, annotated, and used to train the algorithm (Fig. 4C). With this trained algorithm, the robot can automatically navigate the needle to the predetermined starting point on the zebrafish larvae at the chosen angle. While MDA-MB-231 cells were predominantly used, other cancer cell types and clinical patient samples were also tested to validate these injections.

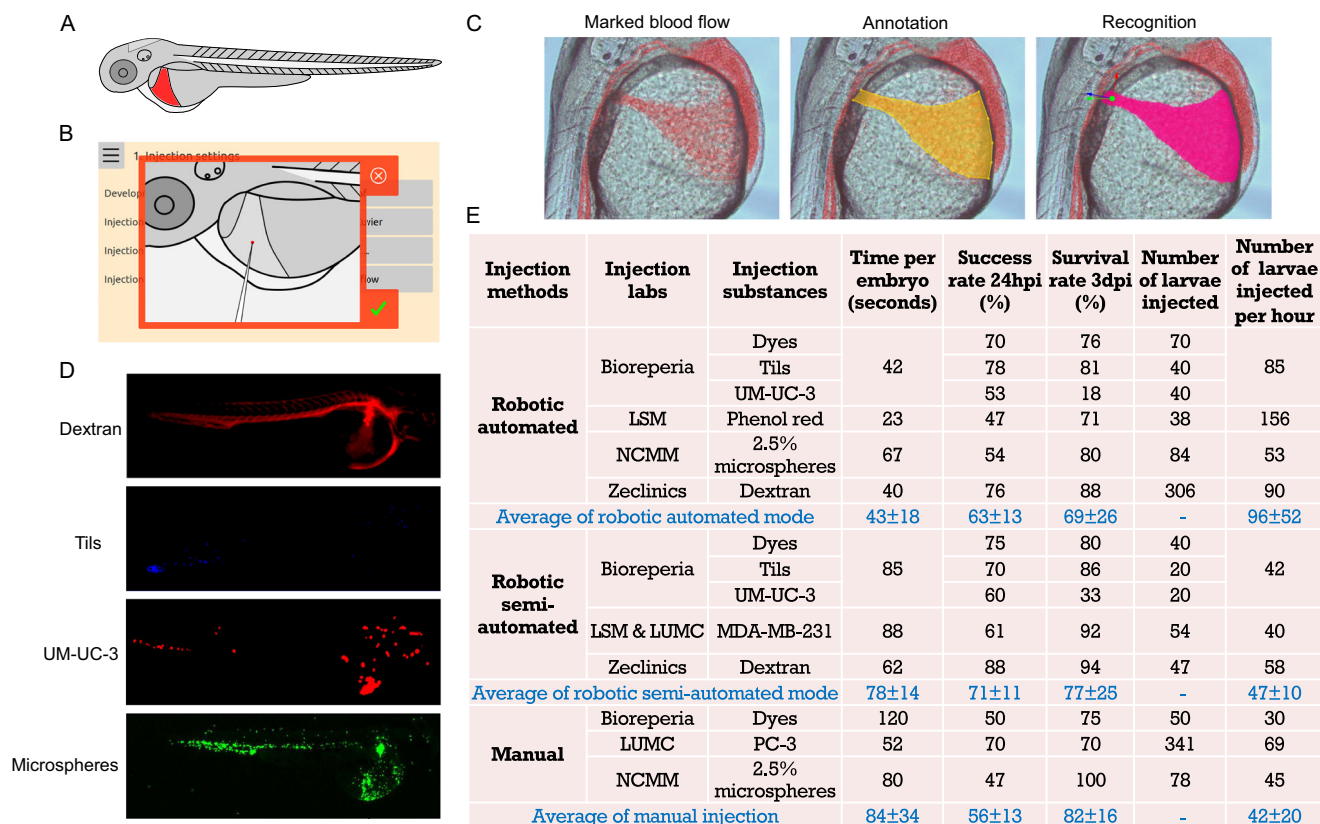


Fig. 3 | Injections into the duct of Cuvier (DoC) of zebrafish larvae. A Schematic illustration of 2 days post-fertilization (dpf) zebrafish larvae, highlighting the targeted DoC area. B Screenshot showing the needle angle and precise positioning of the needle tip for robotic DoC injections. C Representative images demonstrating marked blood flow of 2 dpf larvae, annotation of the DoC, and recognition of the DoC by the robot after algorithm training on thousands of annotated images of DoC. D Fluorescent images displaying the distribution of various substances within the bloodstream at 4 h post-injection (hpi). TILs tumor-infiltrating lymphocytes.

E Comprehensive data on the testing and validation of robotic DoC injections using different substances, with two robotic injection modes, conducted across multiple laboratories. Manual injections using micromanipulators were performed by different researchers for comparison to the robotic injections. The numbers in the average rows represent the mean value ± standard deviation (STDEV). There is no significant difference in the average values between the robotic automated mode and the manual mode. Blue en dash: not applicable.

Robotic automated and semi-automated injections of MDA-MB-231 cells into the PVS of 2 dpf zebrafish larvae are shown in Supplementary Movies 11 and 12, respectively. For cell injections, the needle often becomes partially clogged, affecting the number of cells delivered. To ensure the desired cell number, the macro allows for multiple injection times, and users can stop the injections once the appropriate volume of cells has been delivered (Supplementary Movie 11). Breast cancer cells were effectively delivered into the PVS at 4 h post-injection (hpi) (Fig. 4D and Supplementary Movie 13). Cell migration was observed at 3 days post-injection (dpi). The quantification data of the three different injection methods for the PVS injections in multiple labs is presented in Fig. 4E. For the automated mode, the success rate of MDA-MB-231 cell injections ranged from 39% to 62%. Using the semi-automated mode, the success rate for dyes, UM-UC-3, MDA-MB-231, and clinical samples was between 55% and 80%. With the manual injection method, the success rate for dyes, MDA-MB-231, and the human prostate cancer cell line PC-3 ranged from 70% to 75%. The success rate for HCC1806 cells was relatively low across all three injection methods performed at ZeClinics. Overall, the average injection success rate of the semi-automated mode (60%) was highly comparable to that of the manual methods (63%), while the automated mode had a relatively lower success rate (45%). However, the injection time using the automated mode was half that of the manual approach, allowing for more larvae to be injected within the same timeframe, which can compensate for the lower success rate. In terms of survival rate, the three injection approaches were highly similar, with the exception of a one-time discrepancy observed with MDA-MB-231 cells.

Injections into the hindbrain ventricle of zebrafish larvae

The hindbrain in zebrafish larvae is anatomically located posterior to the midbrain and anterior to the spinal cord (Fig. 5A). For injections into the hindbrain, the needle tip is typically positioned outside the hindbrain between the eye and otic vesicle, so that it punctures into the ventricle (Fig. 5B). To enable the robot to detect the edge of the hindbrain, the borders of images of 2 dpf zebrafish larvae were annotated (Fig. 5C). Additionally, the starting point and direction of the needle were annotated and trained to ensure automatic positioning at the predetermined site and angle (Fig. 5D). Injection of the human GFP-labeled H3K27M-mutant diffuse midline glioma (DMG) cell line (SU-DIPG-XIII-P*) into the hindbrain ventricle resulted in cells being localized in the ventricle at 1-hour post-injection (hpi) and 4-day post-injection (dpi) (Fig. 5E). The injection macro was developed after numerous manual injections and was optimized and validated by NCMM and LSM. In the automated macro mode, the robot will automatically place the needle, execute the macro, and perform the injection upon detecting the edge of the larvae (Supplementary Movie 14). In the semi-automated macro mode, it requires clicking the macro in the manual interface, allowing flexibility for adjustments if needed (Supplementary Movie 15). Double injection times are incorporated into the macro to achieve the desired number of cells for the H3K27M-mutant DMG cell line (Supplementary Movie 15). The quantification data using the two robotic modes was recorded at NCMM for injection of H3K27M-mutant DMG cells and at LSM for injection of the dye phenol red (Fig. 5F). The success rates for dye and H3K27M-mutant DMG cell injections using the automated macro mode were similar (58% vs 57%). These rates were slightly

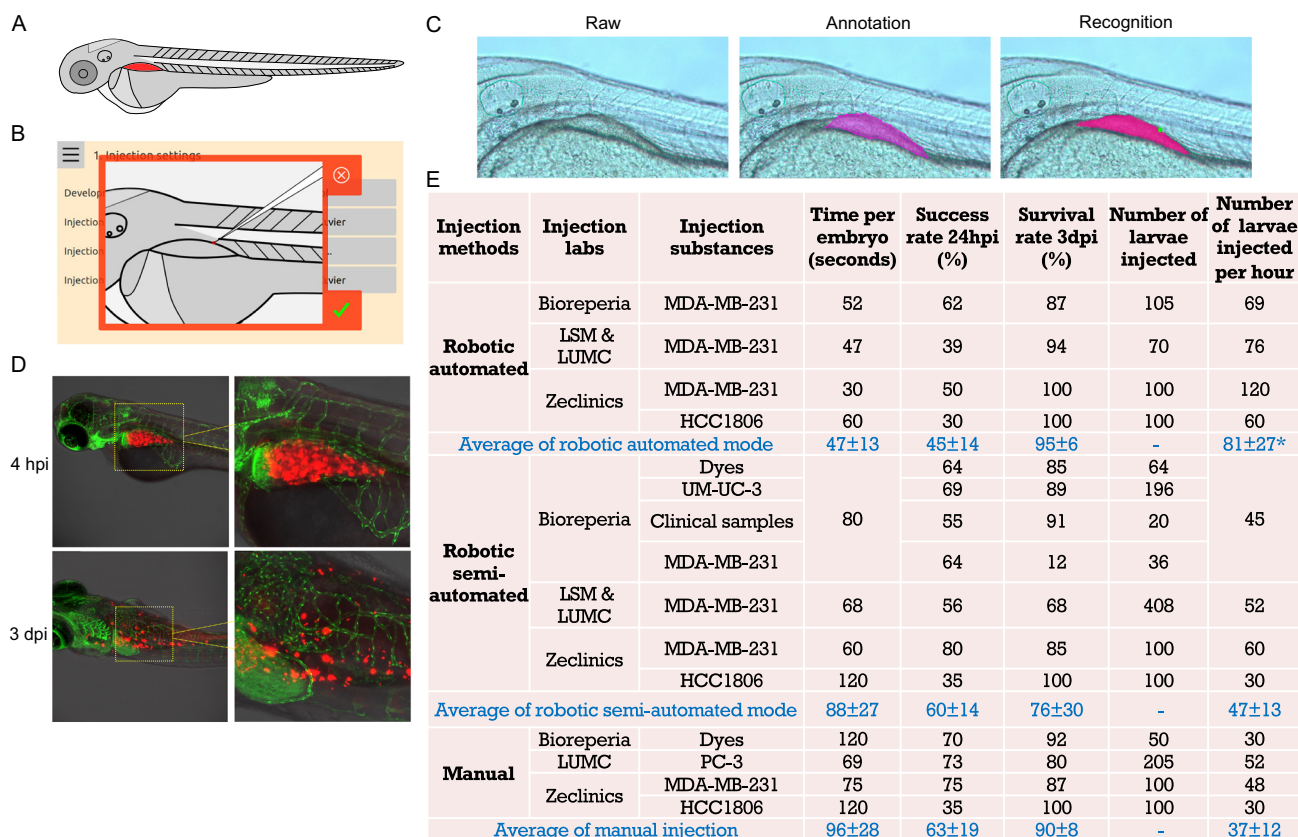


Fig. 4 | Injections into the perivitelline space (PVS) of zebrafish larvae.

A Schematic illustration of 2 days post-fertilization (dpf) zebrafish larvae, highlighting the targeted PVS area. **B** Screenshot depicting the angle and precise positioning of the needle tip for robotic PVS injections. **C** Representative images showing the raw images of the PVS of 2 dpf zebrafish larvae acquired by the robot, annotation of the PVS, and recognition of the PVS by the robot after algorithm training on thousands of annotated PVS images. The green dot on the recognized image indicates the positioning of the needle tip. **D** Fluorescent images displaying mCherry MDA-MB-231 cells in the PVS at 4 h post-injection (hpi), and cell migration at

3 days post-injection (dpi). **E** Comprehensive data on the testing and validation of robotic PVS injections using different cancer cell lines and clinical samples, with two robotic injection modes, conducted across multiple laboratories. Manual injections using a micromanipulator were performed in comparison to the robotic injections. The numbers in the average rows represent the mean value ± standard deviation (STDEV). * $p < 0.05$, the average number of larvae injected per hour in robotic automated mode compared to the average of manual injection. There are no significant differences in the average values of other columns between the robotic automated mode and the manual mode. Blue en dash: not applicable.

lower than those achieved using the semi-automated macro mode (63%) and with manual injection (66%) for H3K27M-mutant DMG cells. However, the injection time of H3K27M-mutant DMG cells for the robotic automated macro mode was approximately half compared to the robotic semi-automated macro mode (120 vs 56 larvae/h) and manual injection (120 vs 57 larvae/h). All injection modes demonstrated high survival rates at 24 hpi (90–95%) (Fig. 5F).

Discussion

In this study, we have developed and introduced a microinjection robot for zebrafish larvae. Utilizing recorded users' best practices, combined with machine learning, macros were developed for fully automated injections into three locations: the DoC, the perivitelline space, and the hindbrain ventricle. The robot can be used in automated or semi-automated mode: The automated mode offers high speed, minimal human interference, and a relatively high success rate, while the semi-automated mode provides flexibility for more insight and development of new injection sites via a user-friendly touchscreen interface. The efficiency of the robot has been tested and validated with various substances by different operators in multiple independent laboratories across Europe. These broad tests help us to identify any lab-specific biases or limitations and ensure the system's reliability, adaptability, and real-world applicability under diverse conditions. The success and survival rates of robotic injections were highly comparable to those of manual injections. Additionally, the automatic injection method offered a significantly faster speed, being twice as fast as

manual injections. Manual microinjection typically requires highly skilled personnel, extensive training, and significant practice to achieve a high success rate. In contrast, operating the robotic system required only a few hours of training, significantly reducing the learning curve and making the technique more accessible.

Intravenous injection is the most common administration route in both mice and human patients. The major vein used for such injections in zebrafish is the DoC. Injections into the DoC have been shown to effectively deliver the injected material throughout the circulatory system³⁷. This method allows researchers to inject cancer cells into the DoC and observe tumor cell dissemination and metastasis in real time, offering insights that are directly translatable to mammalian models and human conditions³⁸. However, achieving intravenous administration in zebrafish larvae presents significant technical challenges, including the need for clear visibility and automatic recognition of blood flow. The design of the coaxial light source, which generates parallel and low-numerical-aperture (NA) light, significantly increases the depth of field. This improvement makes the zebrafish blood flow visible, allowing the blood flow to be labeled and subsequently annotated and trained with an algorithm model. The trained algorithm greatly facilitates the recognition of the DoC and enables precise intravenous administration. Subcutaneous tumor implantation in mice allows for the development of localized tumors, which can be easily monitored and measured over time^{39,40}. This method provides a controlled environment to study tumor growth, angiogenesis, and

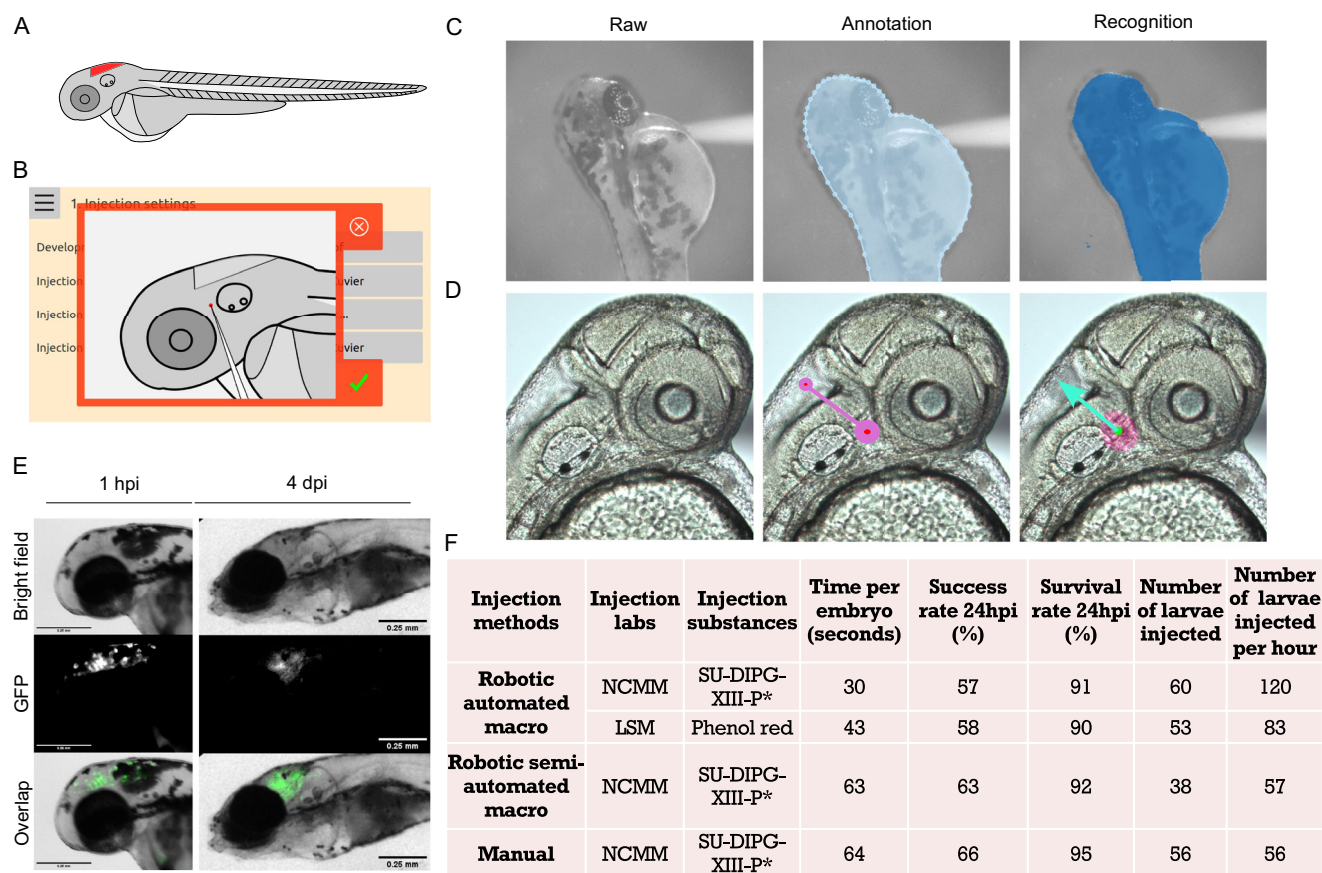


Fig. 5 | Injections into the hindbrain ventricle of zebrafish larvae. **A** Schematic illustration of 2 days post-fertilization (dpf) zebrafish larvae, highlighting the targeted hindbrain ventricle. **B** Screenshot showing the angle and precise positioning of the needle tip for robotic hindbrain injections. **C** Representative images showing the raw images of 2 dpf larvae acquired by the robot, annotation of the larval edges, and recognition of larval shape by the robot after algorithm training on thousands of annotated images. **D** The raw zoomed-in hindbrain images of 2 dpf larvae were acquired using the robot. These images were annotated with a line, where the large pink circle indicates the needle starting point, and the small pink circle indicates the

needle direction. The needle starting point and direction then were recognized by the robot after algorithm training. **E** Images displaying injected GFP-labeled H3K27M-mutant diffuse midline glioma cells (SU-DIPG-XIII-P*) into the hindbrain ventricle at 1-hour post-injection (hpi) and at 4 days post-injection (dpi). **F** Comprehensive data on the testing and validation of robotic hindbrain ventricle injections using phenol red (LSM) and SU-DIPG-XIII-P* cells (NCMM) with two robotic injection modes. Manual injection of SU-DIPG-XIII-P* cells using a micromanipulator was performed as a comparison to the robotic injection modes.

response to therapies⁴¹. The perivitteline space (PVS) in zebrafish larvae is similar to the subcutaneous area in mice, making it a significant site for injections and localized tumor implantations. Micro-injecting cancer cells into the zebrafish PVS is challenging due to its narrowness. In the automatic injection mode, the robotic system detects the needle's skin puncture automatically. Additionally, the subsequent retraction of the needle in the macro ensures proper positioning within the PVS, leading to accurate cell delivery. The zebrafish brain, which is well-developed early in its development, shares the same major structural components as the mammalian brain, including the hindbrain^{42–44}. Hindbrain injections in zebrafish larvae are the most commonly used site for orthotopic implantation of brain tumor cells and for studying tumors that metastasize to the brain⁴⁵. Since the hindbrain is located at the border of a larva, the edge detection design in the injection macro ensures precise needle placement within the hindbrain ventricle, allowing for accurate injection. H3K27M-mutant diffuse midline glioma (DMG) is a high-grade glioma typically diagnosed in children and young adults and preferentially located in the brainstem (pons, midbrain, medulla), thalamus, and spinal cord⁴⁶. Surgical resection is limited due to anatomical location and standard treatment protocols (e.g., chemotherapy) are ineffective, resulting in very poor clinical outcomes with 2-year overall survival rates of 10%⁴⁷. Novel drugs and combination therapies⁴⁸ are hence urgently needed for this patient population and our injection results of H3K27M-mutant

DMG cells into the hindbrain ventricle of zebrafish larvae hold promise for future high-throughput drug screening efforts.

In its current status, the robotic system has proved versatile, effectively handling multiple types of tumor cells, indicating its broad applicability in cancer research. The automation of xenotransplantation procedures not only enhanced precision but also significantly reduced the time required for these procedures, thereby increasing throughput and facilitating large-scale studies. Post-injection analysis confirmed that tumor cells remained viable within the zebrafish larvae, demonstrating successful xenotransplantation and the system's suitability for subsequent research. Retrospective clinical trials have shown promising results, where patient tumor cells were tested in zebrafish xenograft models. These experiments have demonstrated a high correlation (up to 91%) between quantified tumor behavior in zebrafish and patients' responses to standard clinical care for various types of cancers^{13,14,17}. This high level of correlation indicates that xenograft assays offer a promising avenue for personalizing care, potentially reducing suffering and costs associated with multiple types of human cancers. Despite these advantages, the technique currently requires highly skilled personnel and years of practice, making it unsuitable to meet the demands of the number of patients, such as those with colorectal cancer⁴⁹. Our previous work has demonstrated that automation can reduce variability and manual bias while increasing the yield compared to manual microinjections in zebrafish eggs^{50,51}. The zebrafish larvae injection robot presented in this study has the potential to be implemented in diagnostic labs, such as pathology units or

clinical genetics labs, within hospitals. This would enable the decentralization of functional precision medicine, making it accessible to a larger proportion of cancer patients. By integrating such automated systems into clinical workflows, we can enhance the scalability and efficiency of personalized cancer treatments, ultimately improving patient outcomes and expanding the reach of precision medicine.

Additionally, the robotic system offers high versatility in terms of automation across various injection sites, different types of injection applications, and injections in other hosts. Developments are underway for automating injections into alternative sites, such as the caudal vein, swim bladder, and pericardial space. Moreover, the robotic injection system is not limited to zebrafish xenograft models; it can be applied to various other applications, including infectious disease studies, compound screening, and toxicology assays. The system also shows potential for use in other species, such as mosquito egg injections for malaria research. Furthermore, continuous improvements and optimizations are being made to the injection robot to achieve higher success rates and faster speeds, paving the way for more challenging technical solutions in biomedical studies. The advancements in this automated system highlight its potential to transform experimental methodologies and improve the efficiency and scalability of preclinical research.

Methods

Zebrafish breeding and husbandry

Zebrafish were bred and managed in individual labs at Linköping University (supplier of zebrafish embryos to BioReperia), Leiden University, the Norwegian Center for Molecular Medicine (NCMM), and ZeClinics. All breeding and husbandry practices adhered to local animal welfare regulations and followed standard protocols (<http://zfin.org>). We used the wild-type ABTL, the transparent Casper, and the Tg(Fl: GFP) Casper zebrafish lines, the latter of which has GFP-expressing vasculature. In this study, we primarily used zebrafish larvae at the developmental stage of 2 days post-fertilization (dpf) for annotation, machine learning, and injections, as 2 dpf is the most widely used and most suitable stage for these procedures. Nonetheless, we have also tested the hindbrain ventricle injections with 1 dpf zebrafish larvae.

Injection substances

A variety of substances were used for injections, including phenol red (Sigma-Aldrich, #114529), trypan blue (Thermo Fisher, #15250061), and red fluorescent dextran (Thermo fisher scientific, # D1818), the human muscle-invasive urinary bladder cancer cell line UM-UC-3 (ATCC, #CRL-1749), human tumor-infiltrating lymphocytes (TILs, purchased under a special partnership agreement from 4C Biomed), microspheres (Sigma-Aldrich, #L4530), breast cancer cell lines mCherry-labeled MDA-MB-231 (ATCC, HTB-26)), GFP-labeled MDA-MB-231 (gently provided by Dr. Fernanda Raquel da Silva Andrade), mCherry labeled human prostate cancer cell lines PC3 (a kind gift from Dr. Maréne Landström), and GFP-labeled HCC1806 (gently provided by Dr. Fernanda Raquel da Silva Andrade), GFP-labeled H3K27M-mutant diffuse midline glioma cells SU-DIPG-XIII-P* (the primary H3.3K27M-mutant cell line SU-DIPG-XIII-P* was obtained from Dr. Michelle Monje)⁵², and clinical samples from bladder cancer patients. All bladder cancer patient samples were collected with informed consent from the patients and used in this study in accordance with the declaration of Helsinki and following approval from the Swedish Ethical Review Authority (Dnr: 2018_837-32)⁹. TILs range in size from 7 to 15 μm in diameter. The UM-UC-3, MDA-MB-231, PC3, HCC1806, and glioma cells typically have a size range of 15–25 μm . The size range of bladder cancer patient cells falls between 10 and 30 μm . The preparation of these substances was conducted as follows: UM-UC-3, TILs, and clinical samples were prepared at Bioreperia; GFP-labeled HCC1806 was cultured and prepared at ZeClinics; GFP-labeled SU-DIPG-XIII-P* cells were cultured and prepared at NCMM; MDA-MB-231 was cultured and prepared independently at Bioreperia, Leiden University Medical Center (LUMC), and ZeClinics. Human cells were frequently tested for the absence of

mycoplasma, and cell lines were authenticated by short tandem repeat profiling. Cells were incubated under standard cell culture conditions at 37 °C in a humidified incubator with 5% CO₂. The cell culture medium was refreshed every two to three days, and cells were split at appropriate ratios as needed. Cells at 80% confluence were harvested using 0.5% trypsin-EDTA (Biowest, #MS0158100U) or StemPro Accutase (Gibco, #A11105-01) and subsequently washed three times with 1× PBS (VWR, #E403-500). The cells were filtered using a 40–70 μm cell strainer (Corning #352340) before resuspending in either culture medium or 2% polyvinylpyrrolidone 40 (PVP40, Sigma, #102420477) to achieve an approximate density of 2.5×10^8 cells/mL for injection. UM-UC-3 cells were fluorescently labeled using 1,1'-dioctadecyl-3,3,3',3'-tetramethylindocarbocyanine perchlorate (DiI, ThermoFisher, #D3899) according to the manufacturer's instructions. TILs were labeled with 25 μM CellTracker™ Blue CMAC dye (Thermo Fisher, #C2110). SU-DIPG-XIII-P* cells were cultured in DMEM/F-12 basal medium (Gibco, #11330032) supplemented with 1% B-27 Supplement (50X) Minus Vitamin A (Gibco, #12587-010), 1% Penicillin/Streptomycin (Gibco, #151400122), 0.1% Heparin (StemCell Technologies, #7980), 0.02% Epidermal Growth Factor (EGF, Shenandoah Biotechnology, #SHBT100-26), and 0.02% human recombinant Fibroblast Growth Factor (FGF, Shenandoah Biotechnology, #SHBT100-146). SU-DIPG-XIII-P* cells were kept in suspension and treated with StemPro Accutase Cell Dissociation Reagent (Gibco, #A11105-01). Approximately 3×10^6 SU-DIPG-XIII-P* cells/mL were pelleted at 300×g for 5 min and resuspended in 25 μL PBS to achieve a final concentration of approximately 40,000 cells/ μL for injection into hindbrain ventricles. Cryopreserved biopsies from bladder cancer patients were treated and prepared for injection following previously described methods⁹.

Injection preparations

A 1.5% agarose gel was prepared by melting 1.5 g of agarose (Sphaero, #D00247) in 100 mL of egg water followed by pouring the solution into the square plate provided with the robot by LSM, ensuring that the surface of the plate is fully covered. The prepared injection substances were mixed, and 5–8 μL were transferred to individual glass capillary needles using micro-loader tips. For injections of dyes or small-sized cells (e.g., TILs), needles with a tip diameter of 5–10 μm were used. For injections of larger cells (e.g., MDA-MB-231), needles with a tip diameter of 20 μm were used. Both commercial needles (Clunbury Scientific LLC, #B100-58-6, #B100-58-20) and manually pulled needles from borosilicate glass microcapillaries (Harvard apparatus, 30-0038) were utilized in this study. The manually made needles were opened under a microscope before loading them onto the robot. Approximately 2 min prior to implantation, zebrafish larvae were anesthetized in 40 $\mu\text{g}/\text{mL}$ tricaine (Sigma, #E10521-50). Anesthetized zebrafish larvae were placed randomly on the agarose gel plate, ensuring no contact between larvae, and excess water was removed. Excess water is removed because it causes the larvae to move, affecting the accuracy of the puncture. However, even after removing the excess water, a small amount of water remains around the larvae, keeping them moist. Larvae should not stay on the plate for too long (more than 10 min); otherwise, they will dry out, significantly increasing their mortality rate. Therefore, we suggest keeping the injection time per batch within 7 min and adding about 20 larvae per plate for each injection batch. The plate with the anesthetized larvae was placed on the right plate holder of the stage in preparation for injection.

Image annotation and deep learning algorithms

For the automatic detection of larvae and injection sites, deep learning networks were employed. Numerous images of ABTL and Casper zebrafish larvae were collected using the scanning function in the robot's injection interface. These images, including those of the zebrafish larvae and specific injection sites, were annotated using an annotation tool developed by LSM. Using this tool, different regions of a larva were marked with a class (segmentation). In a postprocessing step, an overlap of classes was resolved by choosing a final class for every pixel in the image. For example, if a pixel was

annotated as both “larva” and “eye”, then we chose “eye” as the final class as it provides more specific information.

The annotated images were then used to train a deep-learning network. For image segmentation tasks, we used a U-Net network topology⁵³. We used as input an array of shape $W \times H \times C$ (width \times height \times number of color channels), and as a result an array of shape $W \times H \times N$ (width \times height \times number of classes). During the inference phase, i.e., after the network has been trained and is being used to drive decisions, each of the $W \times H$ pixels in the input image is assigned a predicted class. This is done by selecting the position of the highest value from a vector of the N computed values.

For detecting the moment of puncture of the skin we use a classification network. A classification network typically takes an entire image as input and produces a single class as output. We used the Inception v3 network⁵⁴ as the main vehicle. For each task, whether segmentation or classification, a portion of the annotated images served as training data, while the remaining images were used for validation during the training phase. Wet lab, real, experiments were performed to select the model with the best performance. If the performance was poor, more images were recorded and annotated, and the relevant networks were re-trained on a larger dataset. Automated image augmentation⁵⁵ was used to artificially increase the number of training images.

For training, we used a Shuttle desktop PC with an Intel(R) Core(TM) i9-9900, 64GB of memory, and 1TB SSD combined with an NVIDIA GTX 1070 with 8GB memory. Since a U-Net can occupy a lot of computer memory, it was often necessary to divide the images into smaller images and combine the segmentations back into a larger segmentation. Most training took overnight for testing and multiple days for deployment. Here, it is important to note that a U-Net tends to make mistakes near the edge of its input since less information is available in a neighborhood near the edge than in the center of the image. Therefore, when combining multiple smaller segmentations (304 pixels in width and height), it turned out to be advantageous to overlap them by 50 pixels in both directions.

We found another improvement by observing that while the U-Net can make mistakes, it produces different results when its input is transformed in various ways. We chose 6 trivial transformations that are rotations by multiples of 90° and reflections. During inference, for each of the transformations, the input image is transformed, and a segmentation is computed, which is then transformed back. Then, for each pixel in the resulting six segmentations, a consensus is computed based on the six computed classes for that pixel.

Deep learning methods are only the first step in the decision-making process of the robot. We will now outline briefly how segmentation and classification are used to inject into the DoC of a zebrafish larva using the following steps:

1. The plate is scanned globally using the bottom camera; each image is segmented using a U-Net, where the eyes, yolk, body and swim bladder (or perivitelline space) of each larva are recognized.
2. The centroids of the eyes, yolk and swim bladder are computed.
3. A skewed (non-orthogonal) coordinate system is constructed from these points.
4. Using the user-defined coordinates (as expressed in this coordinate system) we move to the global area of the DoC.
5. Using the top camera, we take multiple, more detailed images at the same location and we combine these images into an image that reveals the blood flow in that area. In this operation, we take the difference between two subsequent images, take the absolute value for every pixel, add these results, and normalize to obtain the final image showing the blood flow. This blood flow is then colored red and overlaid onto the last image of the set.
6. This image is then segmented using another U-Net, where the DoC area is recognized.
7. Since the U-Net can produce mistakes, more than one area can be found. We choose the area which has the most pixels.

8. Using the previously found coordinate system and the segmentation, the needle is moved to the part of the DoC as selected by the user.
9. The robot now adjusts the liquid lens to focus far below the needle, and the system moves the needle down towards the sample while recording images with the top camera.
10. Using a classical algorithm, the sharpness of the images is tracked. When the sharpness reaches a local maximum, the descent of the needle is stopped.
11. The liquid lens is now adjusted to focus just below the needle, the camera selects a smaller field of view, and the needle is moved down in smaller steps. When a sudden increase in sharpness is detected (i.e., a threshold value is reached), the system assumes that the needle is touching the surface.
12. Deep learning is used to detect puncturing with the needle, as follows:
13. If the stage moves in X and Y while the manipulator moves down, then the net effect can be achieved that the needle is moving along its length with respect to the larva.
14. While moving along the length of the needle, a stream of grayscale images is recorded with the top camera.
15. For each triplet of subsequent images, a new image is constructed having three channels.
16. A deep learning classification network that has been trained on these images is used to determine the moment when the needle punctures the skin. To train this network, we annotated the moment of puncture in a similar stream of images, and we used the image triplets as input to the training algorithm.
17. After the skin is punctured, the robot quickly moves the needle out slightly along its length to reduce the likelihood of damage, reduce pressure, and reduce possible obstructions near the tip of the needle, allowing a substance to be injected.
18. An air-pressure pulse is given, and the injection is performed.

Automated injection mode

In the fully automated mode, the robot performs the injections autonomously. The robot scans the agarose gel plate from top to bottom to locate a larva. Upon detecting a larva, the robot approaches it and positions the needle at the predetermined injection sites. The robot then executes a macro tailored to each injection site (Supplementary Movies 8, 11, and 14). After completing the injection, the robot resumes scanning for the next larva.

Semi-automated injection mode

In the semi-automated mode, users have the flexibility to control and adjust the injection process. The robot scans the plate and navigates the needle to the predetermined injection site of a larva. A manual interface appears, allowing users to adjust needle rotation, focus, magnification, injection pressure, and back pressure and to move the needle (Supplementary Movies 9 and 12). Additionally, users can activate the injection macro by clicking the “m” button, which automates the injection while maintaining flexibility (Supplementary Movie 14).

Manual injections

Manual injections are conducted using a pneumatic picopump or femtojet 4 \times and a manipulator. The specific procedures for manual injections into the DoC and PVS have been previously described in detail⁵⁶.

Microscope imaging

Transfer the injected zebrafish larvae to petri dishes containing egg water. If cells were injected, the larvae were maintained in an incubator at 33 °C; otherwise, they were kept at 28.5 °C. In Bioreperia, LUMC, and NCMM, images of injected zebrafish larvae from all injection sites were acquired at 1 to 4 hours post-injection (hpi) using a stereo fluorescent microscope. Additionally, larvae from PVS and hindbrain injections were also imaged at 3 days post-injection (dpi) and 4 dpi, respectively. In ZeClinics, larvae from DoC and PVS injections were imaged at 1–4 hpi using the VAST Bioimager

system (Union Biometrica, US), and the images were subsequently reconstructed into three-dimensional videos.

Statistical analysis

The average performance of the robotic automated mode was compared to that of manual injection. Statistical analysis was performed using a one-tailed test and type 3 (two-sample unequal variance). A *p*-value of less than 0.05 was regarded as significant.

Data availability

Data recorded during injections, and video data, are available on request from the corresponding author. Example recordings are included in the manuscript's supplementary files. The results of injections were analyzed and summarized and these results are published in the tables of the article. The clinical samples used in this study are described in detail in a previous publication <https://doi.org/10.3390/cells12030508>⁹.

Code availability

Source code, annotation and training data developed during this study are proprietary and owned by Life Science Methods.

Received: 19 September 2024; Accepted: 20 February 2025;

Published online: 23 April 2025

References

- Liu, S. & Leach, S. D. *Zebrafish Models for Cancer*. <https://doi.org/10.1146/annurev-pathol-011110-130330> (2011).
- Choi, T. Y., Choi, T. I., Lee, Y. R., Choe, S. K. & Kim, C. H. Zebrafish as an animal model for biomedical research. *Exp. Mol. Med.* **53**, 310–317 (2021).
- Gamble, J. T., Elson, D. J., Greenwood, J. A., Tanguay, R. L. & Kolluri, S. K. The zebrafish xenograft models for investigating cancer and cancer therapeutics. *Biol. (Basel)* **10**, 252 (2021).
- Chen, X., Li, Y., Yao, T. & Jia, R. Benefits of zebrafish xenograft models in cancer research. *Front. Cell Dev. Biol.* <https://doi.org/10.3389/fcell.2021.616551> (2021).
- Somasagara, R. R. & Leung, T. C. Zebrafish xenograft model to study human cancer. in *Methods in Molecular Biology* 2413 45–53 (Humana Press Inc., 2022).
- Fazio, M., Ablain, J., Chuan, Y., Langenau, D. M. & Zon, L. I. Zebrafish patient avatars in cancer biology and precision cancer therapy. *Nat. Rev. Cancer* **20**, 263–273 (2020).
- Xu, W. et al. Characterization of prostate cancer cell progression in zebrafish xenograft model. *Int. J. Oncol.* **52**, 252–260 (2018).
- Drabsch, Y., He, S., Zhang, L., Snaar-Jagalska, B. E. & ten Dijke, P. Transforming growth factor- α signalling controls human breast cancer metastasis in a zebrafish xenograft model. *Breast Cancer Res.* **15**, 1–13 (2013).
- Kowald, S. et al. Novel zebrafish patient-derived tumor xenograft methodology for evaluating efficacy of immune-stimulating BCG therapy in urinary bladder cancer. *Cells* **12**, 508 (2023).
- Fontana, C. M. & Van Doan, H. Zebrafish xenograft as a tool for the study of colorectal cancer: a review. *Cell Death Dis.* **15**, 23 (2024).
- Pliakopanou, A. et al. Glioblastoma research on zebrafish xenograft models: a systematic review. *Clin. Transl. Oncol.* **26**, 311–325 (2024).
- Basheer, F., Dhar, P. & Samarasinghe, R. M. Zebrafish models of paediatric brain tumours. *Int. J. Mol. Sci.* **23**, 9920 (2022).
- Costa, B. et al. Zebrafish Avatar-test forecasts clinical response to chemotherapy in patients with colorectal cancer. *Nat. Commun.* **15**, 4771 (2024).
- Barroso, M. T. et al. Establishment of pancreatobiliary cancer zebrafish avatars for chemotherapy screening. *Cells* **10**, 2077 (2021).
- Lindahl, G. et al. Zebrafish tumour xenograft models: a prognostic approach to epithelial ovarian cancer. *NPJ Precis. Oncol.* **8**, 53 (2024).
- Ali, Z. et al. Zebrafish patient-derived xenograft models predict lymph node involvement and treatment outcome in non-small cell lung cancer. *J. Exp. Clin. Cancer Res.* **41**, 58 (2022).
- Costa, B. et al. Zebrafish Avatars of rectal cancer patients validate the radiosensitive effect of metformin. *Front. Oncol.* **12**, 862889 (2022).
- Mercatali, L. et al. Development of a patient-derived xenograft (PDX) of breast cancer bone metastasis in a Zebrafish model. *Int. J. Mol. Sci.* **17**, 1375 (2016).
- Pontes, K. C. et al. Evaluation of (fli:GFP) casper zebrafish embryos as a model for human conjunctival melanoma. *Invest. Ophthalmol. Vis. Sci.* **58**, 6065–6071 (2017).
- Konantz, M., Müller, J. S. & Lengerke, C. Zebrafish xenografts for the in vivo analysis of healthy and malignant human hematopoietic cells. *Methods Mol. Biol.* **2017**, 205–217 (2019).
- Cabezas-Sáinz, P., Pensado-López, A., Sáinz, B. & Sánchez, L. Modeling cancer using zebrafish xenografts: drawbacks for mimicking the human microenvironment. *Cells* **9**, 1978 (2020).
- Kawakami, K., Patton, E. E. & Orger, M. *Zebrafish Methods and Protocols Second Edition Methods in Molecular Biology*. <http://www.springer.com/series/7651> (2016).
- Nicoli, S. & Presta, M. The zebrafish/tumor xenograft angiogenesis assay. *Nat. Protoc.* **2**, 2918–2923 (2007).
- Brown, H. K., Schiavone, K., Tazzyman, S., Heymann, D. & Chico, T. J. A. Zebrafish xenograft models of cancer and metastasis for drug discovery. *Expert Opin. Drug Discov.* **12**, 379–389 (2017).
- Drabsch, Y., Snaar-Jagalska, B. E. & Ten Dijke, P. Fish tales: the use of zebrafish xenograft human cancer cell models. *Histol. Histopathol.* **32**, 673–686 (2017).
- Haldi, M., Ton, C., Seng, W. L. & McGrath, P. Human melanoma cells transplanted into zebrafish proliferate, migrate, produce melanin, form masses and stimulate angiogenesis in zebrafish. *Angiogenesis* **9**, 139–151 (2006).
- Gopal, U. et al. Development of a triple-negative breast cancer leptomenigeal disease model in zebrafish. *Cells* **12**, 995 (2023).
- Rudzinska-Radecka, M. et al. The anti-tumoral potential of phosphonate analog of sulforaphane in Zebrafish xenograft model. *Cells* **10**, 3219 (2021).
- Wehmas, L. C., Tanguay, R. L., Punnoose, A. & Greenwood, J. A. Developing a novel embryo-larval zebrafish xenograft assay to prioritize human glioblastoma therapeutics. *Zebrafish* **13**, 317–329 (2016).
- Vagionitis S. & Czopka T. *Visualization and Time-Lapse Microscopy of Myelinating In Vivo in Zebrafish*. 1791 (Springer New York, New York, NY, 2018).
- Xu, Q. *Microinjection into Zebrafish Embryos*. (1999).
- Chi, Z., Xu, Q., Ai, N. & Ge, W. Design and development of an automatic microinjection system for high-throughput injection of zebrafish larvae. *IEEE Trans. Autom. Sci. Eng.* **19**, 3409–3418 (2022).
- Ellett, F. & Irimia, D. Microstructured devices for optimized microinjection and imaging of zebrafish larvae. *J. Vis. Exp.* **2017**, 56498 (2017).
- Zhang, G. et al. Zebrafish larva orientation and smooth aspiration control for microinjection. *IEEE Trans. Biomed. Eng.* **68**, 47–55 (2021).
- Qian, C., Yu, X., Tong, M., Zhuang, S. & Lin, W. Visual-guided solutions in automated zebrafish larva heart micro-injection. *IEEE Robot. Autom. Lett.* **7**, 1395–1402 (2022).
- Guo, Z., Ai, N., Ge, W. & Xu, Q. Design of an automated robotic microinjection system for batch injection of zebrafish embryos and larvae. *Microsyst. Nanoeng.* **10**, 20 (2024).
- Isogai, S., Horiguchi, M. & Weinstein, B. M. The vascular anatomy of the developing zebrafish: an atlas of embryonic and early larval development. *Dev. Biol.* **230**, 278–301 (2001).
- Costa, B., Estrada, M. F., Mendes, R. V. & Fior, R. Zebrafish avatars towards personalized medicine—a comparative review between avatar models. *Cells* **9**, 293 (2020).

39. Zhang, Y. et al. Establishment of a murine breast tumor model by subcutaneous or orthotopic implantation. *Oncol. Lett.* **15**, 6233–6240 (2018).
40. Tomayko, M. M. & Reynolds, C. P. determination of subcutaneous tumor size in athymic (nude) mice*. *Cancer Chemother. Pharmacol.* **24**, 148–154 (1989).
41. Ikeda, W., Sasai, K. & Akagi, T. Imaging window device for subcutaneous implantation tumor. in *Methods in Molecular Biology* 1763 153–163 (Humana Press Inc., 2018).
42. Kozol, R. A. et al. Function over form: Modeling groups of inherited neurological conditions in zebrafish. *Front. Mol. Neurosci.* <https://doi.org/10.3389/fnmol.2016.00055> (2016).
43. Guo, S. Using zebrafish to assess the impact of drugs on neural development and function. *Expert Opin. Drug Discov.* **4**, 715–726 (2009).
44. Wilson, S. W., Brand, M. & Eisen, J. S. *III. Neural Development Patterning the Zebrafish Central Nervous System* (2002).
45. Maricic, N. et al. Zebrafish as an orthotopic tumor model for retinoblastoma mimicking routes of human metastasis. *Cancers (Basel)* **14**, 5814 (2022).
46. Mackay, A. et al. Integrated molecular meta-analysis of 1,000 pediatric high-grade and diffuse intrinsic pontine glioma. *Cancer Cell* **32**, 520–537.e5 (2017).
47. Hoffman, L. M. et al. Journal of clinical oncology Clinical, Radiologic, Pathologic, and Molecular Characteristics of Long-Term Survivors of Diffuse Intrinsic Pontine Glioma (DIPG): a Collaborative Report From the International and European Society for Pediatric Oncology DIPG Registries. *J. Clin. Oncol.* **36**, 1963–1972 (2018).
48. Kline, C. et al. Upfront biology-guided therapy in diffuse intrinsic pontine glioma: therapeutic, molecular, and biomarker outcomes from PNOC003. *Clin. Cancer Res.* **28**, 3965–3978 (2022).
49. Morgan, E. et al. Global burden of colorectal cancer in 2020 and 2040: incidence and mortality estimates from GLOBOCAN. *Gut* **72**, 338–344 (2023).
50. Cordero-Maldonado, M. L. et al. Deep learning image recognition enables efficient genome editing in zebrafish by automated injections. *PLoS ONE* **14**, e0202377 (2019).
51. Del Prado, J. A. N. et al. Comparing robotic and manual injection methods in zebrafish embryos for high-throughput RNA silencing using CRISPR-RfxCas13d. *Biotechniques* **76**, 185–193 (2024).
52. Venkatesh, H. S. et al. Electrical and synaptic integration of glioma into neural circuits. *Nature* **573**, 539–545 (2019).
53. Ronneberger, O., Fischer, P. & Brox, T. U-net: Convolutional networks for biomedical image segmentation. in *Lecture Notes in Computer Science (including subseries Lecture Notes in Artificial Intelligence and Lecture Notes in Bioinformatics)* 9351 234–241 (Springer Verlag, 2015).
54. Szegedy, C., Vanhoucke, V., Ioffe, S. & Shlens, J. *Rethinking the Inception Architecture for Computer Vision* (2016).
55. Shorten, C. & Khoshgoftaar, T. M. A survey on Image Data Augmentation for Deep Learning. *J. Big Data* **6**, 1–48 (2019).
56. Li, C. et al. Establishment of embryonic zebrafish xenograft assays to investigate TGF- β family signaling in human breast cancer progression. in *Methods in Molecular Biology* 2488 67–80 (Humana Press Inc., 2022).
- Society (#254836). We extend our sincere thanks to Dr. Maréne Landström, Dr. Fernanda Raquel da Silva Andrade, and Dr. Michelle Monje for generously providing the cell lines used in this study. We also express our deep appreciation to the caretakers in the fish facilities for their dedicated care of the zebrafish.

Author contributions

J.d.S. conceptualized and designed the robotic system. K.J.v.d.K. developed the control hardware, software, and machine learning algorithms for the robot. Y.D., J.H., M.K., and K.J.v.d.K. carried out the image annotations. Y.D., K.J.v.d.K., W.v.d.E., M.S.d.M., S.Ko., J.H., M.K., V.D.D., and J.d.S. developed, validated, and optimized the injection macros of the robotic system. Y.D., W.v.d.E., M.S.d.M., S.Ko., J.M.V.T., and L.M. performed the robotic injections into the DoC. Y.D., M.S.d.M., S.Ko., J.H., and R.A. performed the robotic injections into the PVS. S.M.W. conceived and designed the glioma study. C.K. provided materials and designed the glioma study. S.Ku. performed glioma cell culture and prepared cells for injection into the hindbrain ventricle. W.v.d.E. and Y.D. performed the robotic injections into the hindbrain ventricle. W.v.d.E., M.S.d.M., S.K., G.M., and L.M. performed the manual injections. J.d.S., L.D.J., C.V.E., and S.D. conceived the project. J.d.S., L.D.J., C.V.E., S.M.W., P.T.D., and V.D.D. supervised the research. Y.D. made figures and videos. Y.D. and J.d.S. wrote the first draft of the paper, with all authors contributing to the critical review and approval of the final version.

Competing interests

Y.D., K.J.v.d.K., and J.d.S. work for a company that commercially exploits the robotic system that is used in this publication. The authors have no other competing interests or relevant affiliations with any organization or entity with the subject matter or materials discussed in the paper apart from those disclosed.

Additional information

Supplementary information The online version contains supplementary material available at <https://doi.org/10.1038/s44385-025-00016-y>.

Correspondence and requests for materials should be addressed to Jan de Sonnevile.

Reprints and permissions information is available at <http://www.nature.com/reprints>

Publisher's note Springer Nature remains neutral with regard to jurisdictional claims in published maps and institutional affiliations.

Open Access This article is licensed under a Creative Commons Attribution 4.0 International License, which permits use, sharing, adaptation, distribution and reproduction in any medium or format, as long as you give appropriate credit to the original author(s) and the source, provide a link to the Creative Commons licence, and indicate if changes were made. The images or other third party material in this article are included in the article's Creative Commons licence, unless indicated otherwise in a credit line to the material. If material is not included in the article's Creative Commons licence and your intended use is not permitted by statutory regulation or exceeds the permitted use, you will need to obtain permission directly from the copyright holder. To view a copy of this licence, visit <http://creativecommons.org/licenses/by/4.0/>.

© The Author(s) 2025

Acknowledgements

We gratefully acknowledge the Eurostars program for supporting our research through the ROBO-FISH grant (Grant Number: E! 114899). S.M.W. was supported by a Pioneer Project grant from the Norwegian Cancer